We are IntechOpen, the world's leading publisher of Open Access books Built by scientists, for scientists

4,800
Open access books available

122,000
International authors and editors

135M
Downloads

Our authors are among the

154
Countries delivered to

TOP 1%
most cited scientists

12.2%
Contributors from top 500 universities

WEB OF SCIENCE™

Selection of our books indexed in the Book Citation Index in Web of Science™ Core Collection (BKCI)

Interested in publishing with us?
Contact book.department@intechopen.com

Numbers displayed above are based on latest data collected.
For more information visit www.intechopen.com

10

Three-Dimensional Lineament Visualization Using Fuzzy B-Spline Algorithm from Multispectral Satellite Data

Maged Marghany
Institute of Geospatial Science and Technology (INSTeG)
Universiti Teknologi Malaysia, UTM, Skudai, Johor Bahru
Malaysia

1. Introduction

A lineament is a linear feature in a landscape which is an expression of an underlying geological structure such as a fault. Typically a lineament will comprise a fault-aligned valley, a series of fault or fold-aligned hills, a straight coastline or indeed a combination of these features. Fracture zones, shear zones and igneous intrusions such as dykes can also give rise to lineaments. Lineaments are often apparent in geological or topographic maps and can appear obvious on aerial or satellite photographs. The term 'megalineament' has been used to describe such features on a continental scale. The trace of the San Andreas Fault might be considered an example. The Trans Brazilian Lineament and the Trans-Saharan Belt, taken together, form perhaps the longest coherent shear zone on the Earth, extending for about 4,000 km. Lineaments have also been identified on other planets and their moons. Their origins may be radically different from those of terrestrial lineaments due to the differing tectonic processes involved (Mostafa and Bishta, 2005; Semere and Ghebreab, 2006).

Accurate geological features mapping is critical task for oil exploration, groundwater storage and understanding the mechanisms of environmental disasters for instance, earthquake, flood and landslides. The major task of geologists is documentation of temporal and spatial variations in the distribution and abundance of geological features over wide scale. In this context, the major challenge is that most of conventional geological surveying techniques are not able to cover a wide region of such as desert in the Earth's surface. Quite clearly, to understand the mechanisms generations of geological features and their relationship with environmental disasters such as earthquake, landslide and flood, geological researchers must be able to conduct simultaneous measurements over broad areas of surface or subsurface of the Earth(Novak and Soulakellis 2000 and Marghany et al., 2009a).

This requires the collection of asset of reliable synoptic data that specify variations of critical geological environmental parameters over a wide region for discrete moments. In fact that geological features such as lineament and faults are key parameters that described the Earth generation or disaster mechanisms and significant indicator for oil explorations and

groundwater storages (Semere and Ghebreab, 2006). Fortunately, the application of remote-sensing technology from space is providing geologists with means of acquiring these synoptic data sets.

1.1 Satellite remote sensing and image processing for lineament features detection

Lineaments are any linear features that can be picked out as lines (appearing as such or evident because of contrasts in terrain or ground cover on either side) in aerial or space imagery. If geological these are usually faults, joints, or boundaries between stratigraphic formations. Other causes of lineaments include roads and railroads, contrast-emphasized contacts between natural or man-made geographic features (e.g., fence lines), or vague "false alarms" caused by unknown (unspecified) factors. The human eye tends to single out both genuine and spurious linear features, so that some thought to be geological may, in fact, be of other origins (Semere and Ghebreab, 2006).

In the early days of Landsat, perhaps the most commonly cited use of space imagery in Geology was to detect linear features (the terms "linear" or "photolinear" are also used instead of lineaments, but 'linear' is almost a slang word) that appeared as tonal discontinuities. Almost anything that showed as a roughly straight line in an image was suspected to be geological. Most of these lineaments were attributed either to faults or to fracture systems that were controlled by joints (fractures without relative offsets) (Wang et al. 1990; Vassilas et al. 2002; Robinson et al., 2007).

Lineaments are well-known phenomena in the Earth's crust. Rocks exposed as surfaces or in road cuts or stream outcrops typically show innumerable fractures in different orientations, commonly spaced fractions of a meter to a few meters apart. These lineaments tend to disappear locally as individual structures, but fracture trends persist. The orientations are often systematic meaning, that in a region, joint planes may lie in spatial positions having several limited directions relative to north and to horizontal (Mostafa and Bishta, 2005). Where continuous subsurface fracture planes that extend over large distances and intersect the land surface produce linear traces (lineaments). A linear feature in general can show up in an aerial photo or a space images as discontinuity that is either darker (lighter in the image) in the middle and lighter (darker in the images) on both sides; or, is lighter on one side and darker on the other side. Obviously, some of these features are not geological. Instead, these could be fence lines between crop fields, roads, or variations in land use. Others may be geo-topographical, such as ridge crests, set off by shadowing. But those that are structural (joints and faults) are visible in several ways (Semere and Ghebreab, 2006; Zaineldeen 2011).

Lineament commonly are opened up and enlarged by erosion. Some may even become small valleys. Being zones of weak structure, they may be scoured out by glacial action and then filled by water to become elongated lakes (the Great Lakes are the prime example). Ground water may invade and gouge the fragmented rock or seep into the joints, causing periodic dampness that we can detect optically, thermally, or by radar. Vegetation can then develop in this moisture-rich soil, so that at certain times of year linear features are enhanced. We can detect all of these conditions in aerial or space imagery (Majumdar and Bhattacharya 1998; Katsuaki et al., 1995; Walsh 2000; Mostafa and Bishta, 2005; Semere and Ghebreab, 2006).

Consequently, optical remote sensing techniques over more than three decades have shown a great promise for mapping geological feature variations over wide scale (Mostafa and Bishta, 2005; Semere and Ghebreab, 2006; Marghany et al., 2009a). In referring to Katsuaki et al., (1995); Walsh (2000) lineament information extractions in satellite images can be divided broadly into three categories: (i) lineament enhancement and lineament extraction for characterization of geologic structure;(ii) image classification to perform geologic mapping or to locate spectrally anomalous zones attributable to mineralization (Mostafa et al., 1995; Süzen and Toprak 1998); and (iii) superposition of satellite images and multiple data such as geological, geochemical, and geophysical data in a geographical information system (Novak and Soulakellis 2000; Semere and Ghebreab 2006). Furthermore, remote sensing data assimilation in real time could be a bulk tool for geological features extraction and mapping. In this context, several investigations currently underway on the assimilation of both passive and active remotely sensed data into automatic detection of significant geological features i.e., lineament, curvilinear and fault.

Image processing tools have used for lineament feature detections are: (i) image enhancement techniques (Mah et al. 1995; Chang et al. 1998; Walsh 2000;Marghany et al., 2009b); and (ii) edge detection and segmentation (Wang et al. 1990; Vassilas et al. 2002; Mostafa and Bishta 2005). In practice, researchers have preferred to use the spatial domain filtering techniques in order to get ride of the artificial lineaments and to verify disjoint lineament pixels in satellite data (Süzen and Toprak 1998). Further, Leech et al., (2003) implemented the band-rationing, linear and Gaussian nonlinear stretching enhancement techniques to determine lineament populations. Won-In and Charusiri (2003) found that High Pass Filter enhancement technique provides accurate geological map. In fact, the High Pass filter selectively enhances the small scale features of an image (high frequency spatial components) while maintaining the larger-scale features (low frequency components) that constitute most of the information in the image.

Majumdar and Bhattacharya (1998) and Vassilas et al. (2002), respectively have used Haar and Hough transforms as edge detection algorithms for lineament detection in Landsat-TM satellite data. Majumdar and Bhattacharya (1998) reported that Haar transform is proper in extraction of subtle features with finer details from satellite data. Vassilas et al. (2002), however, reported that Hough transform is appropriate for fault feature mapping. Consequently, Laplacian, Sobel, and Canny are the major algorithms for lineament feature detections in remotely sensed data (Mostafa and Bishta 2005; Semere and Ghebreab, 2006; Marghany 2005).Recently Marghany and Mazlan (2010) proposed a new approach for automatic detection of lineament features from RADARSAT-1 SAR data. This approach is based on modification of Lee adaptive algorithm using convolution of Gaussian algorithm.

1.2 Problems for geological features extraction from remote sensing data

Geological studies are requiring standard methods and procedures to acquire precisely information. However, traditional methods might be difficult to use due to highly earth complex topography. Regarding the previous prospective, the advantage of satellite remote sensing in its application to geology is the wide coverage over the area of interest, where much accurate and useful information such as structural patterns and spectral features can

be extracted from the imagery. Yet, abundance of geological features are not be fully understood. Lineaments are considered the bulk geological features which are still unclear in spite of they are useful for geological analysis in oil exploration. In this sense, the lineament extraction is very important for the application of remote sensing to geology. However the real meaning of lineament is still vague. Lineaments should be discriminated from other line features that are not due to geological structures. In this context, the lineament extraction should be carefully interpreted by geologists.

1.3 Hypothesis of study

Concerning with above prospective, we address the question of uncertainties impact on modelling Digital Elevation Model (DEM) for 3-D lineament visualization from multispectral satellite data without needing to include digital elevation data. This is demonstrated with LANDSAT-ETM satellite data using fuzzy B-spline algorithm (Marghany and Mazlan 2005 and Marghany et al., 2007). Three hypotheses are examined:

- lineaments can be reconstructed in Three Dimensional (3-D) visualization;
- Canny algorithm can be used as semiautomatic tool to discriminate between lineaments and surrounding geological features in optical remotely sensed satellite data; and
- uncertainties of DEM model can be solved using Fuzzy B-spline algorithm to map spatial lineament variations in 3-D.

2. Study area

The study area is located in Sharjah Emirates about 70 Km fromSharjah city. It is considered in the alluvium plain for central area of UAE and covers an Area of 1800 Km^2 (60 km x 30 km) within boundaries of latitudes 24^o 12′N to 24^o.23'N and longitudes of 55^o.51'E to 55^o 59' E (Fig. 1). The northern part of UAE is formed of the Oman mountains and the marginal hills extends from the base of the mountains and (alluvium plain) to the south western sand dunes (Figs 2 and 3) such features can be seen clearly in Wadi Bani Awf, Western Hajar (Fig.2). Land geomorphology is consisted of structural form, fluvial, and Aeolian forms(sand dunes). According to Maged et al., (2009) structural form is broad of the Oman mountains and JabalFayah (Fig.4) which are folded structure due collusion of oceanic crust and Arabian plate (continental plate). Furthermore, the mountain is raised higher than 400 m above sea level and exhibit parallel ridges and high–tilted beds. Many valleys are cut down the mountains, forming narrow clefts and there are also intermittent basins caused by differential erosion. In addition, the Valley bases are formed small caves. Stream channels have been diverted to the southwest and they deposited silt in the tongue -shaped which lies between the dunes. Further, Aeolian forms are extended westwards from the Bahada plain, where liner dunes run towards the southwest direction in parallel branching pattern (Fig. 3) with relative heights of 50 meters. Nevertheless, the heights are decreased towards the southeast due to a decrease in sand supply and erosion caused by water occasionally flowing from the Oman mountains. Moreover, some of the linear dunes are quite complex due to the development of rows of star dunes along the top of their axes. Additionally, inter dunes areas are covered by fluvial material which are laid down in the playas formed at the margins of the Bahadas plain near the coastline. The dunes changes their forms to low flats of marine origin and their components are also dominated by bioclastics and quartz sands (Marghany and Mazlan 2010).

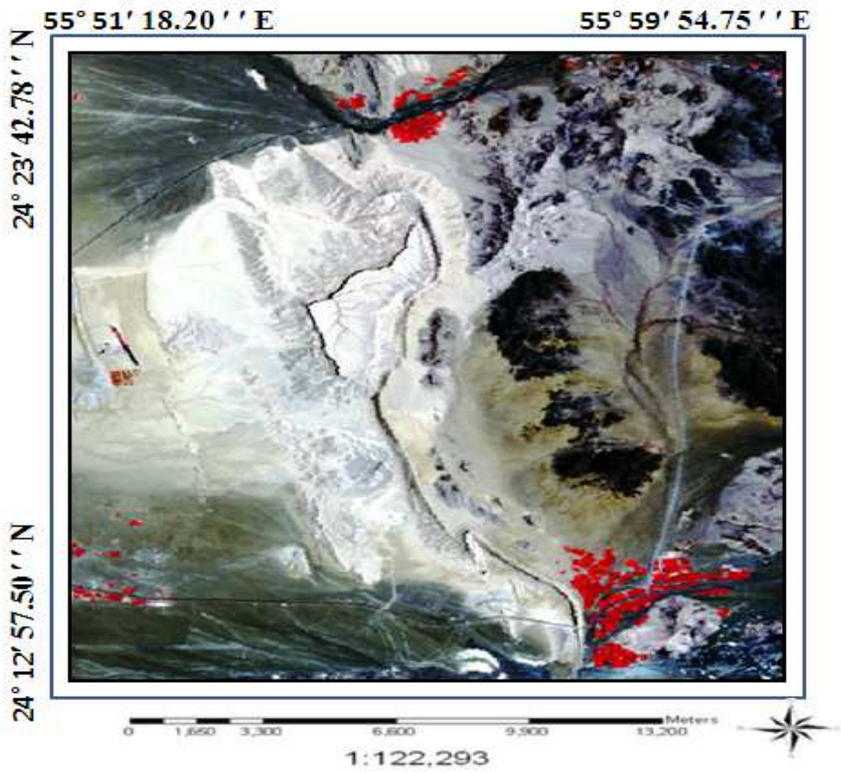

Fig. 1. Location of Study area.

Fig. 2. Geologic fault feature along Oman mountain.

Fig. 3. Dune forms on Oman mountain base.

Fig. 4. Sand dune feature along Jabal Fayah.

3. Data sets

In study, there are two sort of data have been used. First is satellite data which is involved LANDSAT Enhanced Thematic Mapper (ETM) image with pixel resolution of 30 m which is acquired on 14:07, 18 December 2004 (Fig.5). It covers area of 24° 23′ N, 55° 52′ E to 24° 17′ N and 55° 59′ E (Fig.5). Landsat sensors have a moderate spatial-resolution. It is in a polar, sun-synchronous orbit, meaning it scans across the entire earth's surface. With an altitude of 705 kilometres +/- 5 kilometres, it takes 232 orbits, or 16 days, to do so. The satellite weighs 1973 kg, is 4.04 m long, and 2.74 m in diameter. Unlike its predecessors, Landsat 7 has a solid state memory of 378 gigabits (roughly 100 images). The main instrument on board Landsat 7 is the Enhanced Thematic Mapper Plus (ETM+).

The main features of LANDSAT-7 (Robinson et al., 2007) are

- A panchromatic band with 15 m (49 ft) spatial resolution (band 8).
- Visible (reflected light) bands in the spectrum of blue, green, red, near-infrared (NIR), and mid-infrared (MIR) with 30 m (98 ft) spatial resolution (bands 1-5, 7).
- A thermal infrared channel with 60 m spatial resolution (band 6).
- Full aperture, 5% absolute radiometric calibration.

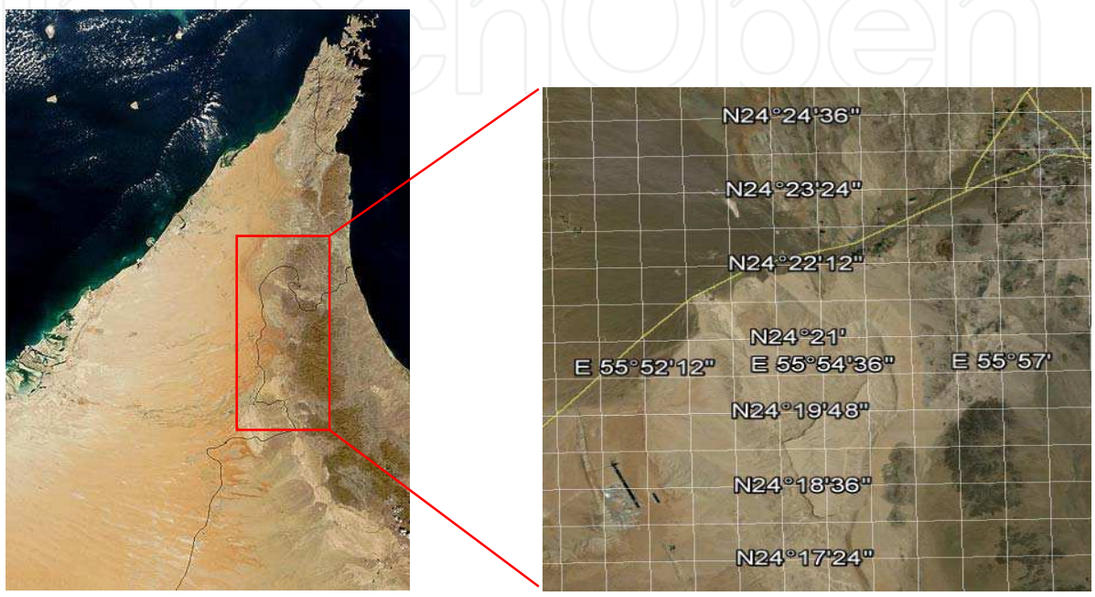

Fig. 5. LANDSAT satellite data used in this study

Second is ancillary data which are contained digital topographic, geological maps, well logs and finally ground water data. Furthermore, ancillary data such as topography map of scale 1: 122,293 used to generate Digital Elevation Model (DEM) of selected area. Bands 1,2,3,5 and 7 are selected to achieve the objective of this study. According to Marghany et al., (2009) these bands can provide accurate geological information. Finally, the Digital Elevation Model (DEM) is acquired from SRTM data (Fig.6).

4. Model for 3-D lineament visualization

The procedures have been used to extract lineaments and drainage pattern from LANDSAT ETM satellite image were involved image enhancement contrast, stretching and linear enhancement which were applied to acquire an excellent visualization. In addition, automatic detection algorithm Canny are performed to acquire excellent accuracy of lineament extraction (Mostafa et al., 1995). Two procedures have involved to extract lineaments from LANDSAT ETM data. First is automatic detection by using automatic edge detection algorithm of Canny algorithm. Prior to implementations of automatic edge detection processing, LANDSAT ETM data are enhanced and then geometrically corrected. Second is implementing fuzzy B-spline was adopted from Marghany et al., (2010) to reconstruct 3D geologic mapping visualization from LANDSAT ETM satellite data.

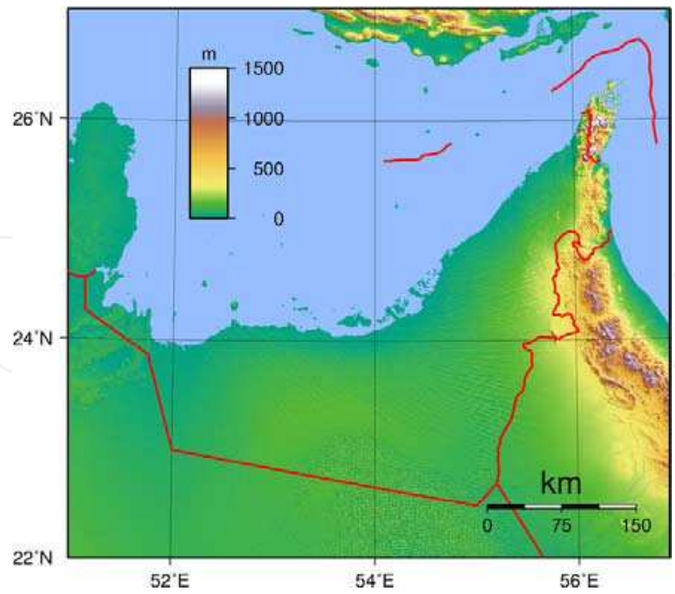

Fig. 6. Topographic map of United Arab Emirates that created with GMT from SRTM data

4.1 Histogram equalization

Following Marghany et al., (2009) histogram equalization is applied to LANDSAT TM image to obtain high quality image visualization. An image histogram is an analytic tool used to measure the amplitude distribution of pixels within an image. For example, a histogram can be used to provide a count of the number of pixels at amplitude 0, the number at amplitude 1, and so on. By analyzing the distribution of pixel amplitudes, you can gain some information about the visual appearance of an image. A high-contrast image contains a wide distribution of pixel counts covering the entire amplitude range. A low contrast image has most of the pixel amplitudes congregated in a relatively narrow range (Süzen et al., 1998 and Gonzalez and Woods 1992).

4.2 Canny algorithm

According to Canny (1986),the Canny edge detector uses a filter based on the first derivative of a Gaussian, because it is susceptible to noise present on raw unprocessed image data, so to begin with, the raw image is convolved with a Gaussian filter. The result is a slightly blurred version of the original which is not affected by a single noisy pixel to any significant degree. According to Deriche (1987) the edge detection operator (Roberts, Prewitt, Sobel for example) returns a value for the first derivative in the horizontal direction **(G_y)** and the vertical direction **(G_x)**. From this the edge gradient and direction (Θ) can be determined:

$$|G| = \sqrt{G_x^{\,2} + G_y^{\,2}} \tag{1}$$

In fact, equation 1 is used to estimate the gradient magnitude (edge strength) at each point can be found to find the edge strength by taking the gradient of the image. Typically, an approximate magnitude is computed using

$$|G| = |G_x| + |G_y| \tag{2}$$

Equation 2 is faster to be computed.

$$\theta = \arctan\left(\frac{G_y}{G_x}\right) \tag{3}$$

The direction of the edge θ is computed using the gradient in the G_x and G_y directions. However, an error will be generated when sum X is equal to zero. So in the code, there has to be a restriction set whenever this takes place. Whenever the gradient (G) in the x direction is equal to zero, the edge direction has to be equal to 90 degrees or 0 degrees, depending on what the value of the gradient in the y-direction is equal to. If G_y has a value of zero, the edge direction will equal 0 degrees. Otherwise the edge direction will equal 90 degrees (Deriche 1987).

According to Gonzalez and Woods (1992),three criteria are used to improve edge detection. The first and most obvious is low error rate. It is important that edges occurring in images should not be missed and that there be NO responses to non-edges. The second criterion is that the edge points be well localized. In other words, the distance between the edge pixels as found by the detector and the actual edge is to be at a minimum. A third criterion is to have only one response to a single edge. This was implemented because the first 2 were not substantial enough to completely eliminate the possibility of multiple responses to an edge (Canny 1986).

4.3 The fuzzy B-splines algorithm

The fuzzy B-splines (FBS) are introduced allowing fuzzy numbers instead of intervals in the definition of the B-splines. Typically, in computer graphics, two objective quality definitions for fuzzy B-splines are used: triangle-based criteria and edge-based criteria (Marghany et al., 2009). A fuzzy number is defined using interval analysis. There are two basic notions that we combine together: confidence interval and presumption level. A confidence interval is a real values interval which provides the sharpest enclosing range for current gradient values.

An assumption μ -level is an estimated truth value in the [0, 1] interval on our knowledge level of the topography elevation gradients (Anile 1997). The 0 value corresponds to minimum knowledge of topography elevation gradients, and 1 to the maximum topography elevation gradients. A fuzzy number is then prearranged in the confidence interval set, each one related to an assumption level $\mu \in [0, 1]$. Moreover, the following must hold for each pair of confidence intervals which define a number: $\mu \succ \mu' \Rightarrow d \succ d'$.

Let us consider a function $f : d \to d'$, of N fuzzy variables $d_1, d_2, ..., d_n$. Where d_n are the global minimum and maximum values topography elevation gradients along the space. Based on the spatial variation of the topography elevation gradients, the fuzzy B-spline algorithm is used to compute the function f (Marghany et al., 2010). Follow Marghany et al., (2010) $d(i,j)$ is the topography elevation value at location i,j in the region D where i is the horizontal and j is the vertical coordinates of a grid of m times n rectangular cells. Let N be

the set of eight neighbouring cells. The input variables of the fuzzy are the amplitude differences of water depth d defined by (Anile et al. 1997):

$$\Delta d_N = d_i - d_0, N = 1, ..., 4 \tag{4}$$

where the d_i, N=1, 4 values are the neighbouring cells of the actually processed cell d_0 along the horizontal coordinate *i*. To estimate the fuzzy number of topography elevation d_j which is located along the vertical coordinate *j*, we estimated the membership function values μ and μ' of the fuzzy variables d_i and d_j, respectively by the following equations were described by Rövid et al. (2004)

$$\mu = \max\left\{\min\left\{m_{pl}(\Delta d_i) : d_i \in N_i\right\}; N = 1...., 4\right\} \tag{5}$$

$$\mu' = \max\left\{\min\left\{m_{LNl}(\Delta d_i) : d_i \in N_i\right\}; N = 1...., 4\right\} \tag{6}$$

Equations 5 and 6 represent topography elevation in 2-D, in order to reconstruct fuzzy values of topography elevation in 3-D, then fuzzy number of digital elevation in *z* coordinate is estimated by the following equation proposed by Russo (1998) and Marghany et al., (2010),

$$d_z = \Delta\mu MAX\{m_{LA}\left|d_{i-1,j} - d_{i,j}\right|, m_{LA}\left|d_{i,j-1} - d_{i,j}\right|\} \tag{7}$$

where d_z fuzzy set of digital elevation values in z coordinate which is function of *i* and *j* coordinates i.e. $d_z = F(d_i, d_j)$. Fuzzy number F_O for water depth in *i,j* and *z* coordinates then can be given by

$$F_O = \{\min(d_{z_0}, ..., d_{z_\Omega}), \max(d_{z_0}, ..., d_{z_\Omega})\} \tag{8}$$

where Ω =1, 2, 3, 4,

The fuzzy number of water depth F_O then is defined by B-spline in order to reconstruct 3-D of digital elevation. In doing so, B-spline functions including the knot positions, and fuzzy set of control points are constructed. The requirements for B-spline surface are set of control points, set of weights and three sets of knot vectors and are parameterized in the *p* and *q* directions.

Following Marghany et al., (2009b) and Marghany et al., (2010), a fuzzy number is defined whose range is given by the minimum and maximum values of digital elevation along each kernel window size. Furthermore, the identification of a fuzzy number is acquired to summarize the estimated digital elevation data in a cell and it is characterized by a suitable membership function. The choice of the most appropriate membership is based on triangular numbers which are identified by minimum, maximum, and mean values of digital elevation estimated. Furthermore, the membership support is the range of digital elevation data in the cell and whose vertex is the median value of digital elevation data (Anile et al. 1997).

5. Three-dimensional lineament visualization

5.1 3-D lineament visulization using classical method

Fig. 4 shows the Digital Elevation Model is derived from SRTM data that covered area of approximately 11 km^2. Clearly, DEM varies between 319-929 m and maximum elevation value of 929 m is found in northeast direction of UAE. Therefore, SRTM has promised to produce DEM with root mean square error of 16 m (Nikolakopoulos et al., 2006). In addition, Oman mountain is dominated by highest DEM value of 929 m which is shown parallel to coastal zone of Arabian Gulf. The DEM is dominated by spatial variation of the topography features such as ridges, sand dunes and steep slopes. As the steep slopes are clearly seen within DEM of 400 m (Fig,7). According to Zaineldeen (2011), the rocks are well bedded massive limestones with some replacement chert band sand nodules. The limestone has been locally dolomitized.

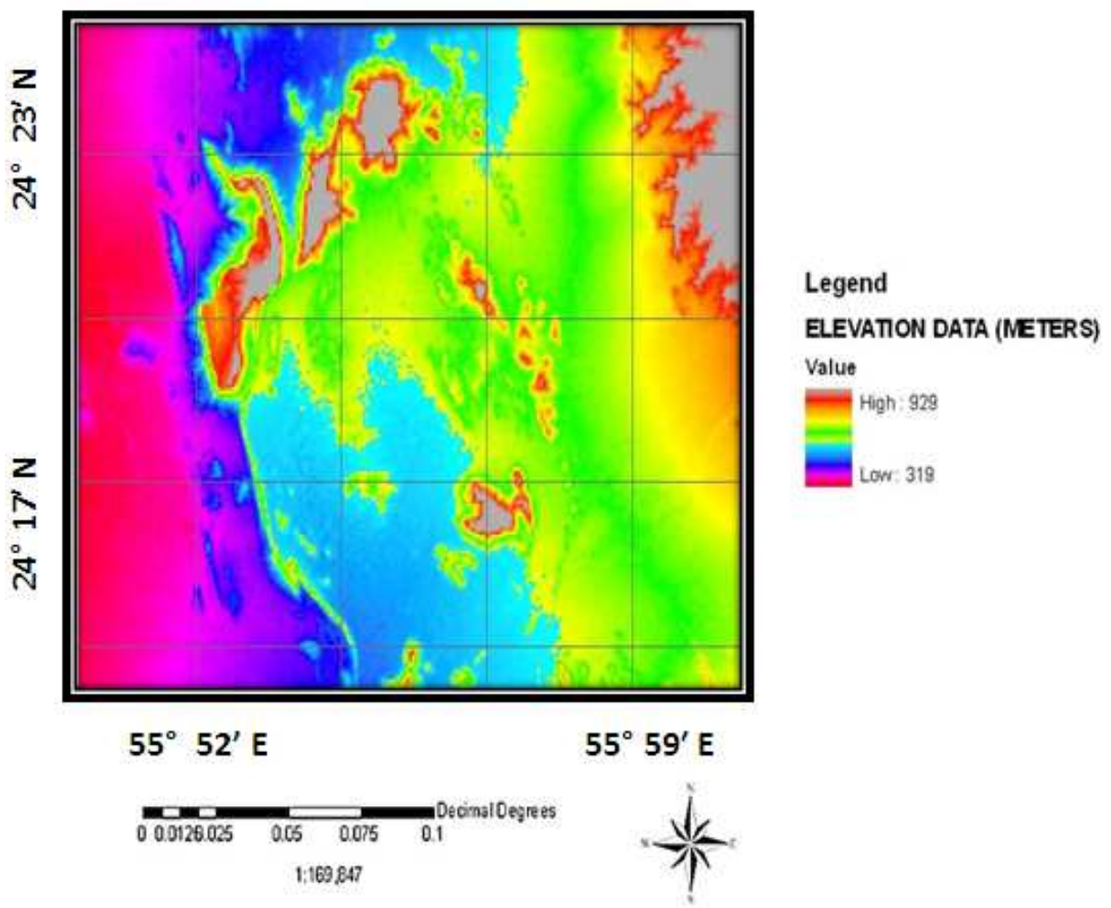

Fig. 7. DEM for study area.

Fig. 8 shows the supervised classification map of LANDSAT ETM satellite data. It clear that the vegetation covers are located in highest elevation as compiled with Fig. 7 while highlands are located in lowest elevation with DEM value of 660 m. The supervised

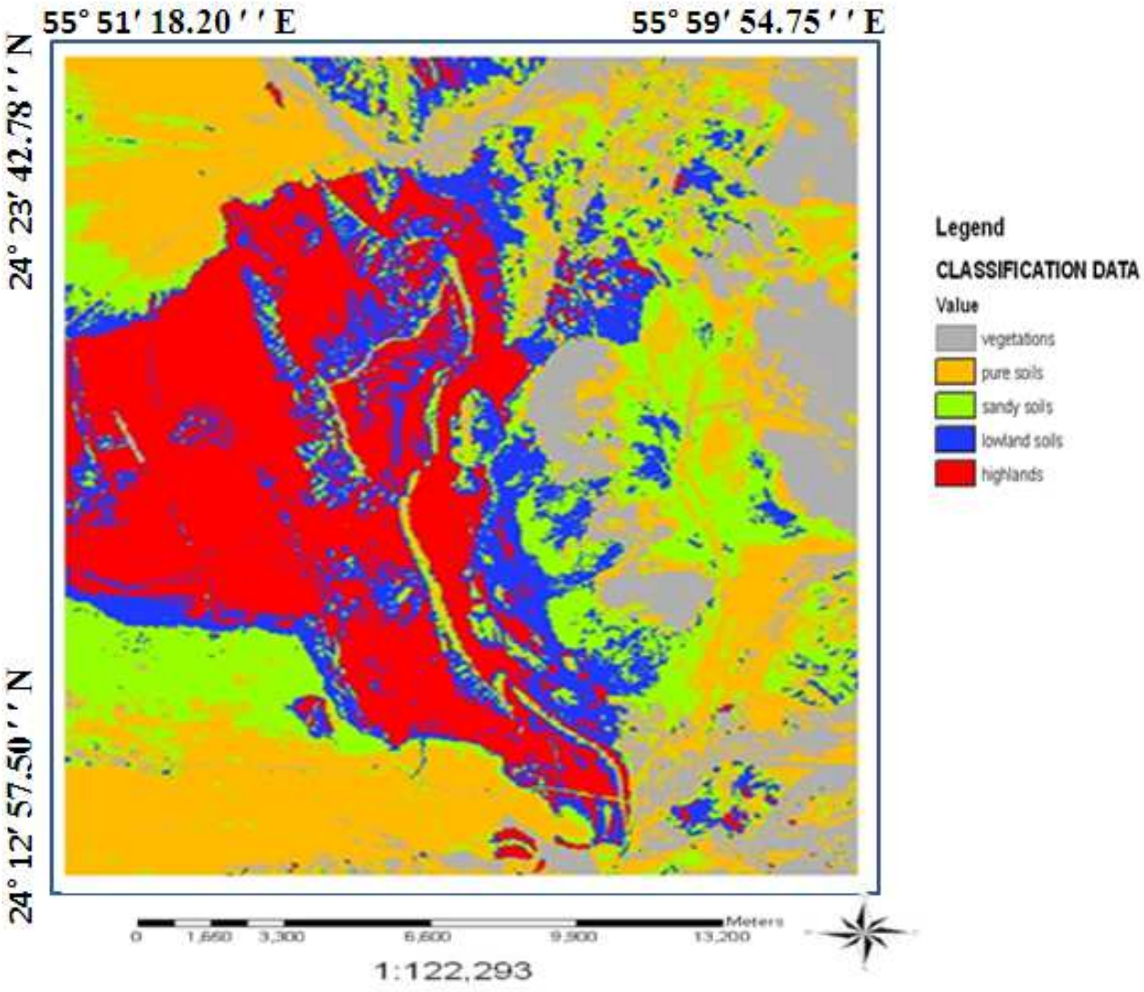

Fig. 8. Supervised map results.

classification shows a great fault moves through a highland area. According to Robinson et al., (2007) , TM bands 7 (2.08–2.35 mm),4 (0.76–0.90 mm),and 2(0.50–0.60 mm)are appropriate for geological features detection because they have low-correlation and produce high-contrast. In this regard, band 2 is useful for rock discrimination, band 4 for land/water contrasts, and band 7 for discrimination of mineral and rock types. Further, TM bands 7 are also able to imagined crest dunes parallel with tens kilometres of length. This feature is clear in northern part of Fig.8 and located in high land of DEM of 900 m. This finding confirm the study of Robinson et al., (2007).

Fig. 9 shows the output result mapping of lineaments using composite of bands 3,4 , 5 and 7 in LANDSAT TM satellite data. The appearance of lineaments in LANDSAT TM satellite image are clearly distinguished. In addition, area adjacent to the mountainous from Manamh (northward), Flili village in the (southward) has high density of lineaments due to the westward compressive force between the oceanic crust and Arabian plate, such as fractures and faults and drainage pattern that running in the buried fault plains (filled

weathered materials coming from Oman mountains) (Fig. 9). The lineaments are associated with fractures and faults which are located in northern part of Fig. 9. In fact that Canny algorithm first is smoothed the image to eliminate and noise. It then finds the image gradient to highlight regions with high spatial derivatives. The algorithm then tracks along these regions and suppresses any pixel that is not at the maximum (non-maximum suppression). The gradient array is further reduced by hysteresis. According to Deriche (1987), hysteresis is used to track along the remaining pixels that have not been suppressed. Hysteresis uses two thresholds and if the magnitude is below the first threshold, it is set to zero (made a non-edge).

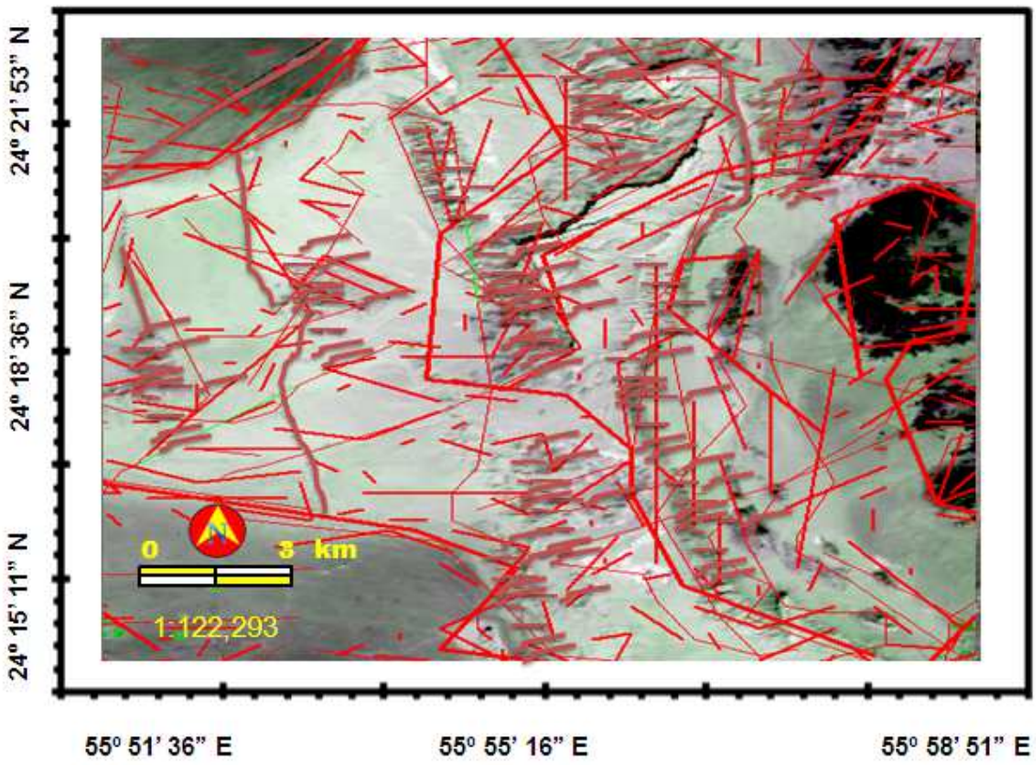

Fig. 9. Lineament mapping using Canny algorithm.

Further, If the magnitude is above the high threshold, it is made an edge. And if the magnitude is between the 2 thresholds, then it is set to zero unless there is a path from this pixel to a pixel with a gradient above threshold. In order to implement the canny edge detector algorithm, a series of steps must be followed. The first step is to filter out any noise in the original image before trying to locate and detect any edges. In fact, the Gaussian filter can be computed using a simple mask, it is used exclusively in the Canny algorithm. Once a suitable mask has been calculated, the Gaussian smoothing can be performed using standard convolution methods. According to Marghany et al., (2009), LANDSAT TM data can be used to map geological features such as lineaments and faults. This could be contributed to that composite of bands 3,4,5 able and 7 in LANDSAT TM satellite data are appropriate for mapping of geologic structures (Katsuaki and Ohmi 1995; Novak and Soulakellis 2000; Marghany et al., 2009). Consequently, the ground

resolution cell size of LANDSAT TM data is about 30 m. This confirms the study of Robinson et al., (2007).

Fig. 10 shows the lineament distribution with 3D map reconstruction using SRTM and LANDSAT TM bands 3,4,5, and 7. It is clear that the 3D visualization discriminates between different geological features. It can be noticed the faults, lineament and infrastructures clearly (Figure 10b). This study agrees with Marghany et al., (2009). It can be confirmed that the lineament are associated with faults and it also obvious that heavy capacity of lineament occurrences within the Oman mountain. This type of lineament can be named as mountain lineament.

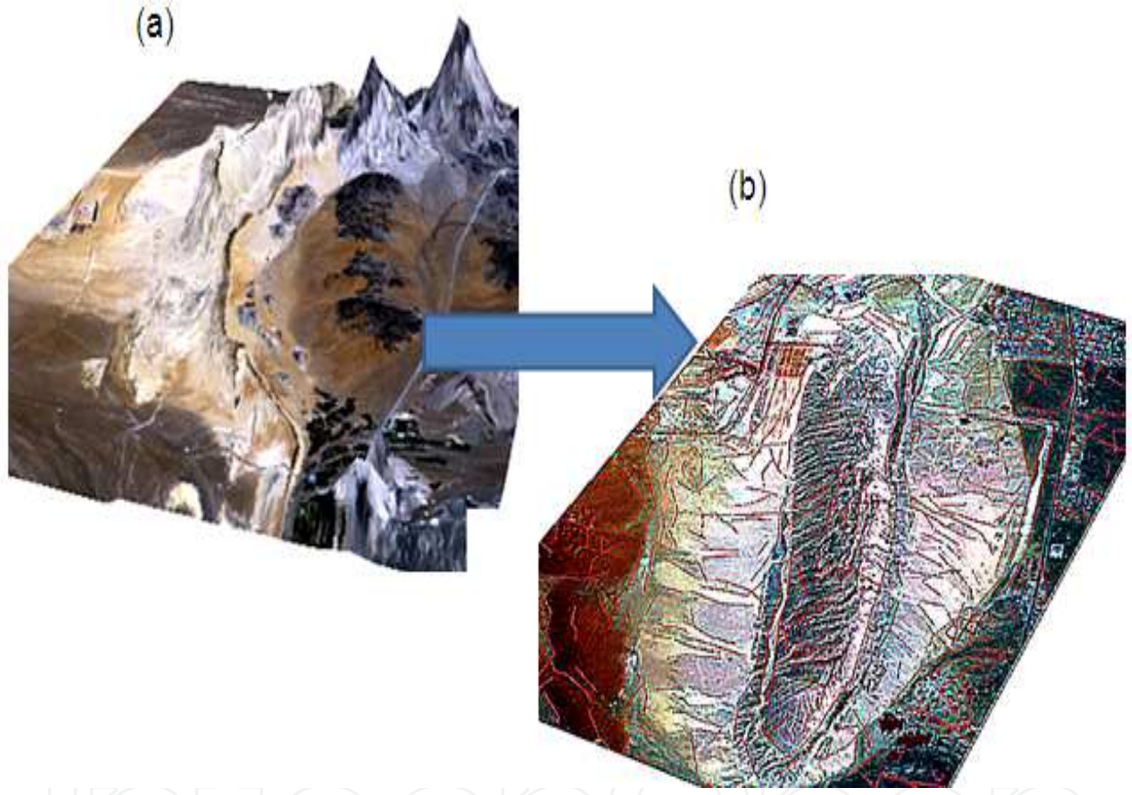

Fig. 10. (a) 3D image reconstruction using SRTM data and (b) lineament distribution over 3D image.

According to Robinson et al., (2007) and Marghany et al., (2009) the mountain is raised higher than 400 m above sea level and exhibit parallel ridges and high-tilted beds. Many valleys are cut down the mountains, forming narrow clefts and small caves. The fluvial forms are consisted of streams channels which are flowed from Oman mountains have and spread out into several braided channels at the base of the mountains from the Bahada and Playa plains (Figure 11). Stream channels have been diverted to the southwest and they deposited silt in the tongue -shaped which lies between the dunes.

Further, Aeolian forms are extended westwards from the Bahada plain, where liner dunes run towards the southwest direction in parallel branching pattern (Fig. 11) with relative heights of 50 meters. Nevertheless, the heights are decreased towards the southeast due to a

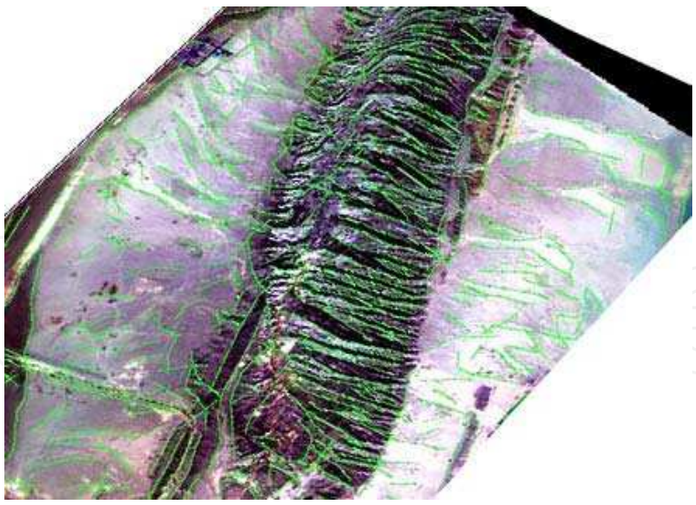

Fig. 11. 3D image and lineament distribution from Canny algorithm.

decrease in sand supply and erosion caused by water occasionally flowing from the Oman mountains. Moreover, some of the linear dunes are quite complex due to the development of rows of star dunes along the top of their axes. Additionally, inter dunes areas are covered by fluvial material which are laid down in the playas formed at the margins of the Bahadas plain near the coastline. The dunes changes their forms to low flats of marine origin and their components are also dominated by bioclastics and quartz sands (Marghany et al., 2009 and Zaineldeen 2011).

5.2 3-D lineament visulization using fuzzy B-spline technique

Fig. 12 shows the result acquires by using fuzzy B-spline algorithm. It is clear that the 3D visualization discriminates between different geological features. It can be noticed the faults, lineament and infrastructures clearly (Fig. 12c). This is due to the fact that the fuzzy B-splines considered as deterministic algorithms which are described here optimize a triangulation only locally between two different points (Fuchs et al., 1977; Anile et al., 1995;Anile, 1997; Marghany et al., 2010; Marghany and Mazlan 2011). This corresponds to the feature of deterministic strategies of finding only sub-optimal solutions usually. The visualization of geological feature is sharp with the LANDSAT TM satellite image due to the fact that each operation on a fuzzy number becomes a sequence of corresponding operations on the respective μ-levels and the multiple occurrences of the same fuzzy parameters evaluated as a result of the function on fuzzy variables Keppel 1975; Anile et al., 1995; Magrghany and Mazlan 2011).

It is very easy to distinguish between smooth and jagged features. Typically, in computer graphics, two objective quality definitions for fuzzy B-splines were used: triangle-based criteria and edge-based criteria. Triangle-based criteria follow the rule of maximization or minimization, respectively, of the angles of each triangle (Fuchs et al., 1977). The so-called max-min angle criterion prefers short triangles with obtuse angles. This finding confirms those of Keppel 1975 and Anile 1997. Table 1 confirms the accurate of fuzzy B-spline to eliminate uncertainties of 3-D visualization. Consequently, the fuzzy B-spline shows higher performance with standard error of mean of 0.12 and bias of 0.23 than SRTM technique. In

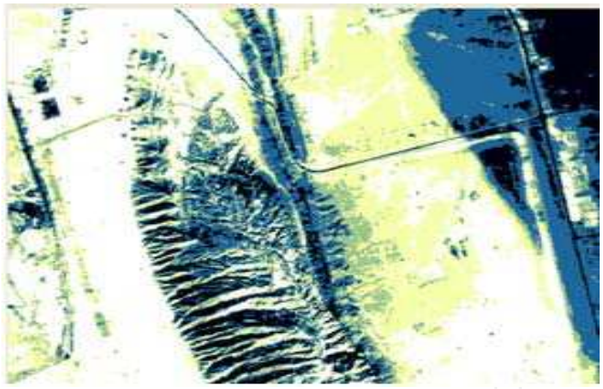

(a)

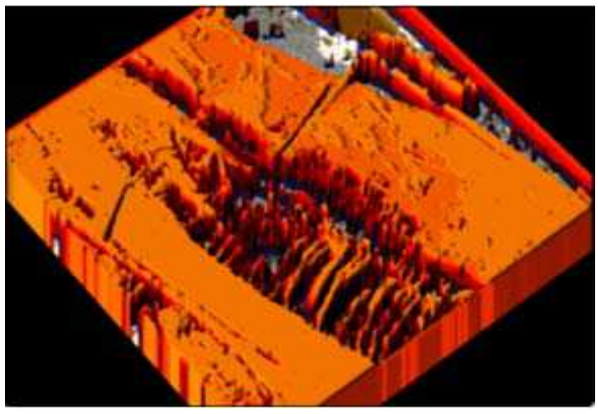

(b)

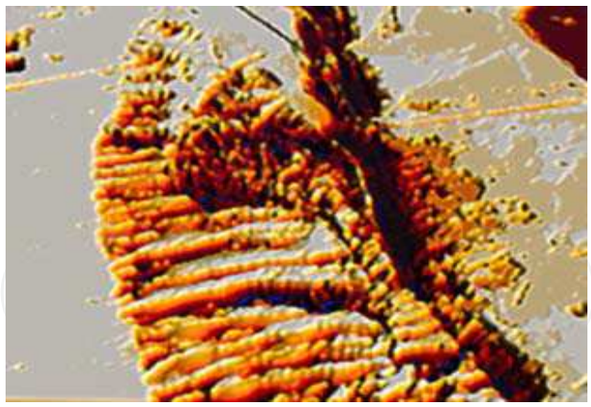

(c)

Fig. 12. (a): LANDSAT ETM satellite data and (b): 3D fuzzy B-spline visualization and (c): Zoom area of lineaments and fault

fact, Fuzzy B-splines provide both a continuous approximating model of the experimental data and a possibilistic description of the uncertainty in such DEM. Approximation with FBS provides a fast way to obtain qualitatively reliable descriptions whenever the introduction of a precise probabilistic DEM is too costly or impossible. In this study, fuzzy B-spline algorithm produced 3-D lineament visulization without need to ground geological

survey. In fact fuzzy B-spline algorithm is able to keep track of uncertainty and provide tool for representing spatially clustered geological features. This advantage of fuzzy B-spline is not provided in Canny algorithm and DEM produced by SRTM data.

Statistical Parameters	3-D Visualization	
	Fuzzy B-spline	SRTM
Bias	0.23	0.63
Standard error of the mean	0.12	0.56

Table 1. Statistical Comparison of 3-D computer visualization using Fuzzy-B-spline and SRTM.

6. Conclusions

This study has demonstrated a method to map lineament distributions in United Arab Emirates (UAE) using LANDSAT-TM satellite data. In doing so, 3D image reconstruction is produced using SRTM data. Then Canny algorithm is implemented for lineament automatic detection from LANDSAT TM bands of 3,4,5,and 7. The results show that the maximum DEM value of 929 m is found in the northeast direction of UAE. The vegetation covers are dominated feature in the highest DEM while highlands are located in lowest elevation of 660 m. In addition, Canny algorithm has detected automatically lineament and fracture features. Therefore, 3D visualization is discriminated between lineament and fault features. The results show that the highest spatial distribution of lineaments are appeared in Oman mountain which are named by lineament mountain. In conclusion, the integration between Digital Elevation Model (DEM) and Canny algorithm can be used as geomatic tool for lineament automatic detection in 3D visualization. Further, a fuzzy B-spline algorithm is used to reconstruct Three Dimensional (3D) visualization of geologic feature spatial variations with standard error of mean of 0.12 and bias of 0.23. In conclusion, combination between Canny algorithm and DEM generated by using fuzzy B-spline could be used as an excellent tool for geologic mapping.

7. References

Anile, A. M, (1997). *Report on the activity of the fuzzy soft computing group*, Technical Report of the Dept. of Mathematics, University of Catania, March 1997, 10 pages.

Anile, AM, Deodato, S, Privitera, G, (1995) *Implementing fuzzy arithmetic*, Fuzzy Sets and Systems, 72,123-156.

Anile, A.M., Gallo, G., Perfilieva, I., (1997). *Determination of Membership Function for Cluster of Geographical data.* Genova, Italy: Institute for Applied Mathematics, National Research Council, University of Catania, Italy, October 1997, 25p., Technical Report No.26/97.

Canny, J., A, (1986). Computational Approach To Edge Detection. IEEE Transactions on Pattern Analysis and Machine Intelligence. PAMI-8 (6), pp. 679-698.

Chang, Y.,Song, G., Hsu, S., (1998). Automatic Extraction of Ridge and Valley Axes Using the Profile Recognition and Polygon-Breaking Algorithm. *Computers and Geosciences*. 24, (1), pp. 83-93.

Deriche, R., (1987). Using Canny's criteria to derive a recursively implemented optimal edge detector. *International Journal of Computer Vision*. 1 (2), pp. 167-187.

Forster, B.C., (1985). Mapping Potential of Future Spaceborne Remote Sensing System. Procs. of 27th Australia Survey Congress, Alice Springs, Institution of Surveyors, Australia, Australia, 109-117.

Fuchs, H. Z.M. Kedem, and Uselton, S.P., (1977). Optimal Surface Reconstruction from Planar Contours. *Communications of the ACM*, 20, 693-702.

Gonzalez, R., and R. Woods (1992).Digital Image Processing, 3rd edition, Addison-Wesley Publishing Company. pp:200-229.

Guenther, G.C., Cunningham, A.G., LaRocque, P. E., and Reid, D. J. (2000). Proceedings of EARSeL-SIG-Workshop LIDAR,Dresden/FRG,EARSeL , Strasbourg, France,June 16 – 17, 2000.

Keppel, E. (1975). Approximation Complex Surfaces by Triangulations of Contour Lines. *IBM Journal of Research Development*, 19, pp: 2-11.

Katsuaki, K., N., Shuichi, and M., Ohmi ,(1995). Lineament analysis of satellite images using a segment tracing algorithm (STA). *Computers and Geosciences*.Vol. 21, No. 9, pp. 1091-I 104.

Leech, D.P., Treloar, P.J., Lucas, N.S., Grocott, J., (2003). Landsat TM analysis of fracture patterns: a case study from the Coastal Cordillera of northern Chile. *International Journal of Remote Sensing*, 24 (19),pp.3709-3726.

Marghany, M., (2005).Fuzzy B-spline and Volterra algorithms for modelling surface current and ocean bathymetry from polarised TOPSAR data. *Asian Journal of Information Technology*. 4, pp: 1-6.

Marghany M., and Hashim, M.,(2006). Three-dimensional reconstruction of bathymetry using C-band TOPSAR data. Photogrammetrie Fernerkundung Geoinformation. pp: 469-480.

Marghay, M., M., Hashim and Crackenal, A., (2007). 3D Bathymetry Reconstruction from AIRBORNE TOPSAR Polarized Data. In: Gervasi, O and Gavrilova, M (Eds.): Lecture Notes in Computer Science. Computational Science and Its Applications – ICCSA 2007, ICCSA 2007, LNCS 4705, Part I, Volume 4707/2007, Springer-Verlag Berlin Heidelberg, pp. 410–420, 2007.

Marghany, M. S., Mansor and Hashim, M., (2009a). Geologic mapping of United Arab Emirates using multispectral remotely sensed data. *American J. of Engineering and Applied Sciences*. 2, pp: 476-480.

Marghany,M., M. Hashim and Cracknell A (2009b). 3D Reconstruction of Coastal Bathymetry from AIRSAR/POLSAR data. *Chinese Journal of Oceanology and Limnology*.Vol. 27(1), pp.117-123.

Marghany, M. and M. Hashim (2010). Lineament mapping using multispectral remote sensing satellite data. *International Journal of the Physical Sciences* Vol. 5(10), pp. 1501-1507.

Marghany, M., M. Hashim and Cracknell A. (2010). 3-D visualizations of coastal bathymetry by utilization of airborne TOPSAR polarized data. *International Journal of Digital Earth*, 3(2):187 – 206.

Mah, A., Taylor, G.R., Lennox, P. and Balia, L., (1995). Lineament Analysis of Landsat Thematic Mapper Images, Northern Territory, Australia. *Photogrammetric Engineering and Remote Sensing*, 61(6),pp. 761-773.

Majumdar, T.J., Bhattacharya, B.B., (1988). Application of the Haar transform For extraction of linear and anomalous over part of Cambay Basin, India. *International Journal of Remote Sensing*. 9(12),pp. 1937-1942.

Mostafa, M.E. and M.Y.H.T. Qari, (1995).An exact technique of counting lineaments. *Engineering Geology*. 39 (1-2), pp. 5-15.

Mostafa, M.E. and A.Z. Bishta, (2005). Significant of lineament pattern in rock unit classification and designation: A pilot study on the gharib-dara area. Northen eastern Desert, Egypt. *International Journal of Remote Sensing*. 26 (7), pp. 1463 – 1475.

Novak, I.D. and N. Soulakellis, (2000). Identifying geomorphic features using Landsat-5/TM data processing techniques on lesvos, Greece. *Geomorphology*. 34: 101-109.

Nikolakopoulos, K. G.; Kamaratakis, E. K; Chrysoulakis, N. (2006). "SRTM vs ASTER elevation products. Comparison for two regions in Crete, Greece". *International Journal of Remote Sensing*. 27 (21), 4819–4838.

Semere, S. and W. Ghebreab, (2006). Lineament characterization and their tectonic significance using Landsat TM data and field studies in the central highlands of Eritrea. *Journal of African Earth Sciences*. 46 (4), pp. 371-378.

Süzen, M.L. and V. Toprak, (1998).Filtering of satellite images in geological lineament analyses: An application to a fault zone in central Turkey. *International Journal of Remote Sensing*. 19 (6), pp. 1101-1114.

Russo, F., (1998).Recent advances in fuzzy techniques for image enhancement. IEEE Transactions on Instrumentation and measurement. 47, pp: 1428-1434.

Robinson, C.A. F.El-Baz, T.M.Kuskyb, M.Mainguet, F.Dumayc, Z.AlSuleimani, A.Al Marjebye (2007). Role of fluvial and structural processes in the formation of the Wahiba Sands, Oman: A remote Sensing Prospective. *Journal of Arid Environments*. 69,676–694.

Rövid, A., Várkonyi, A.R. andVárlaki, P., (2004). 3D Model estimation from multiple images," IEEE International Conference on Fuzzy Systems, FUZZ-IEEE'2004, July 25-29, 2004, Budapest, Hungary, pp. 1661-1666.

Vassilas, N., Perantonis, S., Charou, E., Tsenoglou T., Stefouli, M., Varoufakis, S., (2002). Delineation of Lineaments from Satellite Data Based on Efficient Neural Network and Pattern Recognition Techniques. *2nd Hellenic Conf. on AI, SETN-2002*, 11-12 April 2002, Thessaloniki, Greece, Proceedings, Companion Volume,355-366.

Walsh, G.J. and S.F. Clark Jr., (2000). Contrasting methods of fracture trend characterization in crystalline metamorphic and igneous rocks of the Windham quadrangle, New Hampshire. Northeast. *Northeastern Geology and Environmental Sciences*. 22 (2), pp. 109-120.

Won-In, K., Charusiri, P., (2003). Enhancement of thematic mapper satellite images for geological mapping of the Cho Dien area, Northern Vietnam. *International Journal of Applied Earth Observation and Geoinformation*, Vol. 15, 1-11.

Zaineldeen U. (2011) Paleostress reconstructions of Jabal Hafit structures,Southeast of AlAin City, United Arab Emirates (UAE). *Journal of African Earth Sciences*. 59,323–335

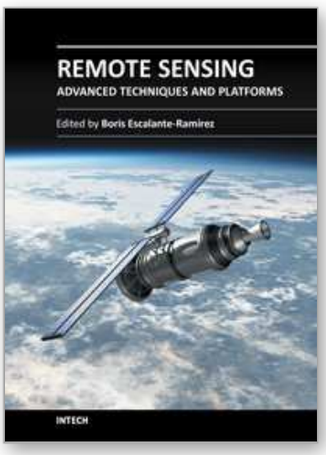

Remote Sensing - Advanced Techniques and Platforms
Edited by Dr. Boris Escalante

ISBN 978-953-51-0652-4
Hard cover, 462 pages
Publisher InTech
Published online 13, June, 2012
Published in print edition June, 2012

This dual conception of remote sensing brought us to the idea of preparing two different books; in addition to the first book which displays recent advances in remote sensing applications, this book is devoted to new techniques for data processing, sensors and platforms. We do not intend this book to cover all aspects of remote sensing techniques and platforms, since it would be an impossible task for a single volume. Instead, we have collected a number of high-quality, original and representative contributions in those areas.

INTECH
open science | open minds

InTech Europe
University Campus STeP Ri
Slavka Krautzeka 83/A
51000 Rijeka, Croatia
Phone: +385 (51) 770 447
Fax: +385 (51) 686 166
www.intechopen.com

InTech China
Unit 405, Office Block, Hotel Equatorial Shanghai
No.65, Yan An Road (West), Shanghai, 200040, China
中国上海市延安西路65号上海国际贵都大饭店办公楼405单元
Phone: +86-21-62489820
Fax: +86-21-62489821

IntechOpen